Exploring Cd-Zn-O-S alloys for improved buffer layers in thin-film photovoltaics

J. B. Varley* and V. Lordi
Lawrence Livermore National Laboratory, Livermore, California 94550, USA

X. He and A. Rockett
Department of Materials Science and Engineering, University of Illinois at Urbana-Champaign, Urbana, Illinois 61801, USA
(Received 7 March 2017; published 17 July 2017)

To compete with existing and more mature solar cell technologies such as crystalline Si, thin-film photovoltaics require optimization of every aspect in the device heterostructure to reach maximum efficiencies and cost effectiveness. For absorbers like CdTe, $Cu(In,Ga)Se_2$ (CIGSe), and $Cu_2ZnSn(S,Se)_4$ (CZTSSe), improving the n-type buffer layer partner beyond conventional CdS is one avenue that can reduce photocurrent losses and improve overall performance. Here, we use first-principles calculations based on hybrid functionals to explore alloys spanning the Cd-, Zn-, O-, and S-containing phase space to identify compositions that may be superior to common buffers like pure CdS or Zn(O,S). We address issues highly correlated with device performance such as lattice-matching for improved buffer-absorber epitaxy and interface quality, dopability, the band gap for reduced absorption losses in the buffer, and the conduction-band offsets shown to facilitate improved charge separation from photoexcited carriers. We supplement our analysis with device-level simulations as parameterized from our calculations and real devices to assess our conclusions of low-Zn and O content buffers showing improved performance with respect to CdS buffers.

DOI: 10.1103/PhysRevMaterials.1.025403

I. INTRODUCTION

Thin-film photovoltaics (PV) offer an attractive route for large-scale and low-cost solar-energy-harvesting technologies, but a number of challenges remain in securing their place over more conventional Si-based solar cells. These primarily include an optimization of the processes and materials used to fabricate the thin-film solar cell heterostructure and represent a much more complex problem compared to the relative simplicity and maturity of Si device fabrication. Of the emerging candidate absorber materials, both CdTe and $Cu(In,Ga)Se_2$ (CIGSe) alloys have recently exceeded 21% efficiency in laboratory devices, while other more earth-abundant alternative absorbers like $Cu_2ZnSn(S,Se)_4$ (CZTSSe) or organometallic perovskites show future promise [1,2].

In conventional CdTe, CIGSe, and CZTSSe devices, an additional layer is incorporated between the absorber and window layers to protect the absorber while facilitating improved charge transport within the solar cell stack. This so-called buffer layer most often consists of chemical bath deposited (CBD) CdS due to its ease of deposition and other favorable properties such as robust n-type conductivity and a favorable band alignment for separation and collection of the photogenerated carriers. The use of CdS buffer layers has repeatedly led to record-setting devices despite it having a room-temperature band gap (∼2.4 eV) that absorbs valuable photons in the blue region of the solar spectrum which are not believed to contribute to the photocurrent [3]. Therefore reducing this absorption and improving the overall collection of the photogenerated carriers offers a clear avenue for the further optimization of CIGSe and CZTSSe PV [3–5]. This approach has already been widely pursued and Cd-free buffers such as Zn(O,S,OH) are an increasingly competitive alternative to CdS, but still represents a constrained choice for an optimal buffer layer.

Here, we consider alloys within the quaternary space formed by Cd, Zn, O, and S to identify solid solution compositions that may provide favorable alternatives to CdS buffer layers in conventional thin-film PV devices. Using hybrid functional calculations, we investigate a number of properties relevant to device performance as a function of the O and Zn content to explore possible alloys that may lead to higher-efficiency devices, and we corroborate the results with device-level simulations. The specific criteria we consider include (1) lattice-match for improved epitaxy as a metric for absorber-buffer interface quality and reduced interfacial hole recombination velocity, (2) larger band gaps that reduce absorption losses, (3) conduction-band offsets relative to the absorber layer that improve both charge collection and dopability, and (4) compositions that can be experimentally realized. We further explore the various combinations of these features that lead to improved device performance parameters, such as the open-circuit voltage (V_{oc}) and the short-circuit current (J_{sc}), using device simulations. Our results identify composition regimes predicted to improve performance over conventional CdS buffers by incorporating small fractions of Zn and O and offer the prospect of grading the buffer and window layers to achieve higher-performing devices.

II. COMPUTATIONAL METHODS

Our calculations are based on density functional theory with the Heyd-Scuseria-Ernzerhof (HSE06) screened hybrid functional [6] and projector-augmented wave (PAW) approach [7] as implemented in the VASP code [8]. The fraction of nonlocal Hartree-Fock exchange (α) in the HSE functional was set to 32% for all alloy calculations, as this value was found to accurately reproduce the band gap of CdS compared to experiment [9,10]. Using these parameters underestimates

*varley2@llnl.gov

 ©2017 American Physical Society

TABLE I. Summary of the lattice constants used for the bulk binary references in the $Cd_{1-x}Zn_xO_yS_{1-y}$ quaternary space for the zinc-blende (a^{zb}) and wurtzite (a^{wz}, c^{wz}) phases. Reference lattice constants (a^{abs}) for CISe, CGSe, CZTS, and CZTSe absorbers relevant for epitaxial growth of zinc-blende buffers on (002) facets (a^{abs}) and wurtzite buffers on the (112) facets ($\sqrt{2}a^{abs}$) are also included [10,15–17].

Material	CdO	CdS	ZnO	ZnS	CISe	CGSe	CZTS	CZTSe
a^{zb} (Å)	5.09	5.89	4.58	5.43	5.78	5.61	5.43	5.69
a^{wz} (Å)	3.62	4.17	3.25	3.83	4.09	3.97	3.84	4.02
c^{wz} (Å)	5.81	6.80	5.22	6.28	–	–	–	–

the band gaps of ZnS and ZnO and overestimates the band gap of CdO compared to values known experimentally and/or reported theoretically using many-body perturbation theory (GW approximation) [11–13], so we evaluate the bulk properties of these materials at α values of 36%, 37.8%, and 27%, respectively. We use linear interpolation to correct the band gaps and band offsets calculated for the alloys, by using the differences obtained with the improved mixing parameter values compared to 32%. The results obtained for the optimized lattice constants and band gaps for the different α values are included in Tables I and II. The lattice constants are in excellent agreement with available bulk experimental values ($<\sim$1%) [14].

We use 64-atom supercells for the zinc-blende alloys based on 32-atom special quasirandom structures (SQS) for each cation and anion face-centered cubic (fcc) sublattice as described elsewhere [18,19]. This yields a set of 289 unique structures that we use to sample the zinc-blende $Cd_{1-x}Zn_xO_yS_{1-y}$ composition space for the properties described below. The lattice constant for each structure was chosen following Vegard's law interpolation between the lattice constants of the four parent phases. Additional details of the alloy calculations can be found in Ref. [19].

We compute band alignments as a function of stoichiometry based on the branch-point energy (E_{BP}) evaluated for each composition, due to the difficulty in uniquely constructing explicit interfaces or surfaces to evaluate the band offsets directly. The branch-point energy, also referred to as the charge-neutrality level (CNL), represents an effective energy where the bulk states change from predominantly valence-band-like or donorlike character to conduction-band-like or acceptorlike character. The concept of the E_{BP} or CNL has had tremendous success in providing a common reference level on which to align the unstrained band edges of semiconductors and insulators [20–27]. While various methods have been proposed to calculate the E_{BP}, we adopt the approach of Schleife *et al.*, which modified previous methodologies for determining this quantity from the bulk electronic structure [25,26]. This procedure defines the E_{BP} as

$$E_{BP} = \frac{1}{2N_{\mathbf{k}}} \sum_{\mathbf{k}} \left[\frac{1}{N_{CB}} \sum_{i}^{N_{CB}} \varepsilon_{c_i}(\mathbf{k}) + \frac{1}{N_{VB}} \sum_{j}^{N_{VB}} \varepsilon_{v_j}(\mathbf{k}) \right], \quad (1)$$

which depends on the eigenvalues ε of the single-particle states, the chosen k-point sampling (i.e., the particular wave vectors $\mathbf{k}$ and their total number $N_{\mathbf{k}}$), the number of included conduction-band states N_{CB}, and valence-band states N_{VB}. For our zinc-blende alloy supercells, we consider all eight irreducible k points comprising the $2 \times 2 \times 2$ Γ-centered k-point mesh. Schleife *et al.* adopted a choice of $N_{VB} = 2$ and $N_{CB} = 1$ for the two-atom zinc-blende unit cell, which we scale to $N_{VB} = 64$ and $N_{CB} = 32$ for our 64-atom alloy supercells [25]. This choice leads to nearly identical results for the bulk supercell for each of CdO, CdS, ZnS, and ZnO compared to E_{BP} determined for the primitive unit cells, as summarized in Table II, thus validating the approach. To correlate the E_{BP} and CNL with an explicitly calculated Fermi-level pinning value, we refer to values we have previously determined for the CdS and ZnS systems in the cation-rich limit desirable for buffer performance [10]. Namely, we identify pinning levels 2.49 and 2.54 eV above the valence-band edge for wurtzite CdS and ZnS, respectively, which fall an average 0.4 eV above the calculated E_{BP} (see Table II). These values were associated with H and O impurities, and so we adopt an estimated Fermi-pinning level 0.4 eV above the calculated E_{BP} values in the subsequent analysis.

We perform device-level simulations with the SCAPS-1D simulation software [28] adopting the material parameters detailed by Frisk *et al.* in Ref. [29]. Our model includes a

TABLE II. Summary of the calculated formation enthalpies (ΔH), band gaps (E_g), and branch-point energies (E_{BP}) relative to the bulk VBM for the binary references in the $Cd_{1-x}Zn_xO_yS_{1-y}$ quaternary space for the zinc-blende and wurtzite phases. All values are obtained with HSE06 using a mixing parameter of $\alpha = 32\%$, while "corrected" values as described in the main text are included for CdO, ZnO, and ZnS in parentheses. The E_{BP} determined for the primitive unit cells and the alloy supercells are both included and indicate relatively small error for consistent scaling of bands. All units are in eV.

Material	CdO	CdS	ZnO	ZnS
ΔH^{zb}	−2.09 (−2.07)	− 1.56	−3.15 (−3.21)	−1.96 (−2.00)
ΔH^{wz}	−2.10 (−2.09)	− 1.57	−3.18 (−3.24)	−1.96 (−2.00)
E_g^{zb}	1.43 (1.14)	2.45	2.87 (3.29)	3.66 (3.87)
E_g^{wz}	1.53 (1.23)	2.52	3.01 (3.43)	3.73 (3.93)
E_{BP}^{zb} (unitcell)	2.51 (2.36)	1.98	3.17 (3.38)	2.11 (2.20)
E_{BP}^{zb} (supercell)	2.53 (2.38)	1.98	3.21 (3.42)	2.10 (2.19)
E_{BP}^{wz} (unitcell)	2.57 (2.42)	1.95	3.29 (3.51)	2.03 (2.13)
E_{BP}^{wz} (supercell)	2.60 (2.44)	1.97	3.32 (3.54)	2.05 (2.15)

double-graded Ga-dependent profile for the CIGSe layer as parameterized from a MiaSolé device and adopts a Ga-dependent defect concentration as in model B from Ref. [29] (also see Ref. [30]). We additionally scale the defect concentration profile such that the maximum concentration does not exceed $2.5 \times 10^{14}\ \mathrm{cm}^{-3}$ in the CIGSe layer, since this value resulted in simulated device performance for our reference samples that more closely matched that obtained in typical experimental devices. Each layer in the stack adopted energy-dependent absorption profiles for each material. For the model buffer layers with different band gaps, we simply translated the CdS absorption profile from an edge at 2.45 eV to the relevant band gap of a given buffer alloy composition.

III. RESULTS AND DISCUSSION

A. Thermodynamic stability

While we investigate a number of material properties in the following sections, the viability of a given alloy composition is ultimately determined by its thermodynamic stability. Our previous studies on the energetics of the quaternary alloys identified that only a narrow range of quaternary solid solution compositions are predicted to be stable for typical PV-processing conditions, largely owing to the low miscibility of oxysulfide solid solutions [19]. For example, at 1000 K, we predicted that the solid solutions would phase separate into highly O-poor and O-rich compositions of less than ~2% and greater than 98% O, respectively [19]. The miscibility of the cation species was found to be far greater than the anion species at a given temperature, with full miscibility of Zn in S-rich samples predicted above ~800 K and above ~1100 K in O-rich samples [19].

We also found that competing phases such as sulfates and sulfites are highly thermodynamically favorable and may nucleate from the regions that exhibit more O-rich (S-poor) compositions. These compounds are known to have large band gaps that would presumably reduce the effective absorption in the buffer, but understanding of their overall affect on the electrical and optical properties of the buffer layers is lacking. We still expect electron transport within the buffer to be dominated by the phases with the lowest-lying conduction bands on an absolute energy scale, which would likely be CdS or a related alloy (see Sec. III F). Considering these facts, we believe that quaternary buffer solid solutions will generally be constrained to the regimes of either low or high O contents for typical photovoltaic growth processes, with more flexibility over the relative Cd and Zn ratios. Nonetheless, we evaluate several key properties related to desirable buffer layer performance over the entire composition space to more clearly identify trends and promising alloy compositions.

B. Properties influencing interfacial recombination

An understanding of how all of the material properties in a solar cell heterostructure interact to influence overall performance is critical to optimizing the device [31]. Recently, Li *et al.* have reported a systematic analysis on various loss mechanisms in state-of-the-art CIGSe devices, such as nonradiative recombination at the absorber-buffer interface, within the space-charge region, and within the absorber bulk, and how these relate to properties within the solar cell [32]. Their study revealed how in typical state-of-the-art devices, the V_{oc} is limited by either interfacial or bulk recombination, which offers a clear path for improving these devices. Additional sensitivity studies by Mangan *et al.* further highlighted routes to improving performance through engineering the buffer layer, where the influence of the carrier concentration, interface quality, and conduction-band offset with the absorber were found to yield a complex parameter space for identifying optimal properties [5].

Insight into the influence of various materials properties on performance can be extracted from the recombination rate coefficient at the interface,

$$R_i = S_h N_v e^{\frac{-\phi_{b0}}{k_{\mathrm{B}} T}}, \tag{2}$$

where S_h represents the hole interface recombination velocity, N_v represents the effective valence-band density of states in the absorber, ϕ_{b0} is the hole potential barrier at the buffer/absorber interface at zero bias, and $k_{\mathrm{B}}T$ is the product of the Boltzmann constant and temperature [32,33]. Modifying the composition of the buffer will alter both S_h and ϕ_{b0}, which each have a distinct influence on performance. S_h is proportional to the density of interfacial defects and their capture cross section and can be minimized by improving the interface quality. ϕ_{b0} is sensitive to the amount of inversion at the interface and intimately depends on both the conduction-band offset (CBO) and the amount of incorporated ionized donors in the buffer and the absorber surface, two properties paramount to optimizing the overall device efficiency [5]. In the following sections, we consider a variety of factors such as the degree of lattice matching, light absorption, and the CBOs of the alloys that can influence these terms and discuss alloy compositions that may minimize losses to the photocurrent and overall device efficiency due to interfacial recombination and parasitic absorption.

C. Lattice matching for improved epitaxy

First, we discuss the influence of alloying on the lattice constant, which offers the possibility of engineering improved epitaxy of $\mathrm{Cd}_{1-x}\mathrm{Zn}_x\mathrm{O}_y\mathrm{S}_{1-y}$ buffer layers deposited on particular absorbers. Identifying lattice-matched buffer alloys would improve the quality of the interface with the absorber and expectedly diminish the S_h term in Eq. (2). Most importantly, the possibility of a high-quality interface could lead to the extraction of useful photocurrent even for photons absorbed within the buffer layer, partially offsetting the desire to identify larger-band-gap buffer candidates. Yet another consequence of improving the lattice-match would decrease the amount of misfit dislocations which may introduce trap states within the band gap and/or influence the band offsets at the heterojunction [34], both of which are critical to controlling the device performance.

Indirect support of these points comes from the high-efficiency (certified 16.3%) commercial flexible CIGSe modules produced by MiaSolé, which have been shown to exhibit remarkable crystalline quality and epitaxy at the absorber-buffer interface [15,35,36]. These studies identified that the CdS buffers grown by physical vapor deposition (PVD) form large epitaxially-grown layers in both cubic and hexagonal modifications with the phase dependent on the exposed CIGSe

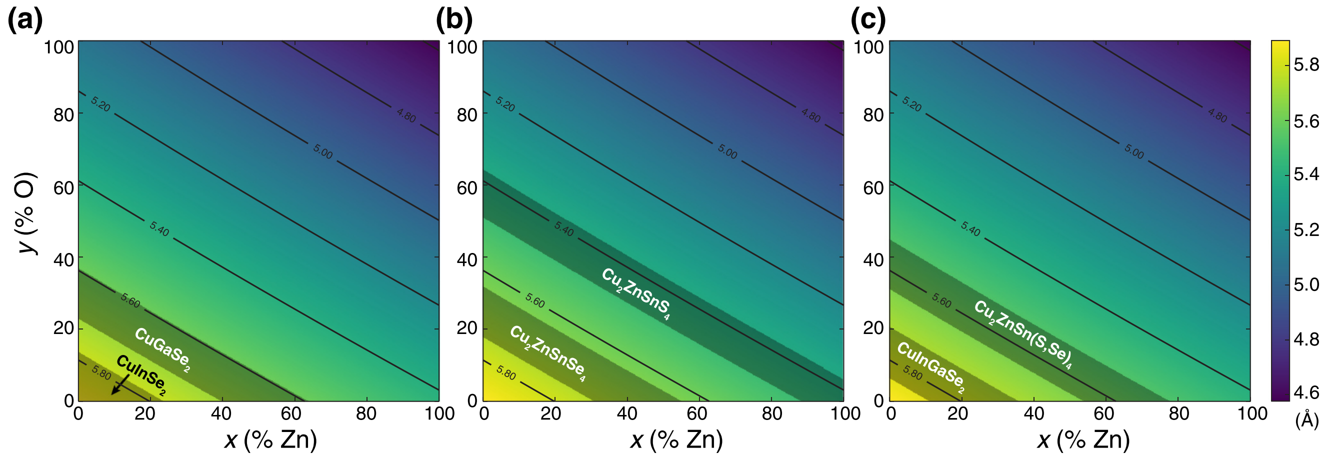

FIG. 1. Lattice constant maps for zinc-blende $Cd_{1-x}Zn_xO_yS_{1-y}$ solid solution shown as a function of the O and Zn content over the quaternary phase space, and assuming Vegard's law. Shaded regions are included in each panel for a reference absorber lattice constant with a tolerance of $\pm 1\%$ lattice mismatch with respect to the buffer using the values in Table I. The shaded references represent the a lattice constants of (a) pure $CuInSe_2$ and $CuGaSe_2$, (b) the emerging absorbers Cu_2ZnSnS_4 and $Cu_2ZnSnSe_4$, and (c) their respective alloys of $CuIn_{0.7}Ga_{0.3}Se_2$ and $Cu_2SnZn(S_{0.4}Se_{0.6})_4$ that yield desirable band gaps of $\sim$1.2 eV. The four corners in each panel represent the bulk lattice constants of CdS (lower left), CdO (upper left), ZnO (upper right), and ZnS (lower right).

facet. He *et al.* find that exposed (112) facets of CIGSe favor the epitaxy of the close-packed planes of the wurtzite CdS buffer with the orientation (0001)‖(112), while the zinc-blende buffers preferentially grow epitaxially on (001) and (110) CIGSe facets and adopt the same corresponding orientation [15]. These observations imply a relationship of $a^{zb} \parallel a^{abs}$ for zinc-blende buffer layers to grow epitaxially on the absorber, and $\sqrt{2}a^{wz} \parallel a^{abs}$ for wurtzite.

To examine how the expected lattice-matching to the absorber could change with composition, we construct a two-dimensional plot of the alloy lattice constants in Fig. 1 assuming Vegard's Law and the calculated lattice constants summarized in Table I for the pure binary buffer compounds. In Fig. 1, we focus on the zinc-blende phase but note that nearly identical conclusions hold for wurtzite based on the close agreement between the buffer lattice constants, a^{zb} and $\sqrt{2}a^{wz}$ (see Table I). We have highlighted several regions of interest that could facilitate improved epitaxy for low or high Ga-content CIGSe or in CZTSSe by incorporating some fraction of O and/or Zn into pure CdS buffers. In each panel, we emphasize the compositions that would yield a lattice match within $\pm 1\%$ of the a^{abs} lattice constant of the various absorbers summarized in Table I, where we assume the same epitaxial relationships would apply between the buffer and kesterite or stannite CZTSSe as they do for the chalcopyrite CIGSe. Considering previous analyses for (110) oriented epitaxial buffer layers on CISe [37], this tolerance would imply a critical thickness of at least ten up to hundreds of monolayers, which is comparable to the thickness of conventional CdS buffers (<$\sim$100 nm) [38].

This analysis neglects the fact that the real CIGSe surfaces tend to exhibit a Cu deficiency that can accommodate doping at the interface [15,39–42], which would lead to a larger effective surface lattice constant for deposited CdS-derived buffers due to the larger size of Cd compared to Cu. Similarly, Zn doping would likely lead to an effective surface lattice constant very comparable to the undoped absorber due to its similar size to Cu. We estimate an increase on the order of 1% in the a^{abs} effective surface lattice constants with respect to undoped CIGSe based on the observed changes in the lattice constant of charge-compensated $Cu_3CdIn_3Se_4$ ($\sim$2% increase from CISe) and $Cu_3CdGa_3Se_4$ ($\sim$3% increase from CGSe) chalcopyrite compounds. We do not include this information explicitly in the shaded regions of Fig. 1, but the overall effect translates the lattice-matched regions toward the origin in Figs. 1(a) and 1(c), i.e., closer to pure CdS. We did not calculate Cd-containing alloys for CZTS and CZTSSe, but the effects would expectedly be similar in these materials.

The plots reveal that pure CdS is most closely lattice-matched to pure CISe, and that the incorporation of Ga in the CIGSe alloys decreases the likelihood for forming a coherent interface consistent with experimentally observed epitaxial relationships [15]. This can, in principle, be overcome by incorporating some fraction of O and/or Zn into pure CdS, which leads to a reduction in the lattice-parameter that can compensate the decreased lattice constant upon the alloying of Ga in the CIGSe. The typical low-Ga content ($\sim$30% Ga) CIGSe is included in Fig. 1(c), where lattice-matching would expectedly occur for Cd(O,S) alloys with $\sim$10% O content, and lower if some amount of Zn is also incorporated. Higher Ga-content CIGSe devices are known to exhibit a higher S_h than low-Ga CIGSe in state-of-the-art devices [32] and would require even more O and/or Zn to achieve better interface quality with CdS-derived buffers. For example, Li *et al.* identified the S_h to be $\sim$3 times larger in the high-Ga content CIGSe devices [32], but the extent to which this difference is due to the quality of the interface versus the influence of intrinsic DX-center defects in the high Ga-CIGSe is not clear and requires further study [43,44].

The importance of improving the quality of the interface in high-Ga CIGSe cells is further substantiated by the fact that S_h limits the V_{oc} and the benefits of the higher-gap absorber are lost for buffers with negative CBOs, so-called "cliff" offsets [31,45]. This same analysis motivates the need to

identify different candidate alloy compositions with a positive CBO, or "spike" offset, for low- or high-Ga CIGSe that can make up for undesirable S_h values. Alternatively, significantly increasing the free carrier concentrations in the buffer through doping can also help offset these effects by moving the p-n junction deeper into the absorber and decreasing the sensitivity of performance to the properties of the interface [5]. Zn(O,S) has emerged as an attractive candidate for improving properties like the conduction-band offset and absorption losses [10,38,42,46], but from Fig. 1, it is expected that these alloys will likely always suffer from a larger S_h than their Cd-containing counterparts.

For CZTSSe, we find pure CdS is very poorly suited for forming the same quality of interface as observed for CIGSe absorbers. This is supported by the much larger interfacial recombination at the CdS/absorber interface in champion CZTSSe versus CIGSe devices [47]. Pure ZnS is found be a much better candidate considering its good match with pure CZTSe, but its performance in CZTSSe devices has been shown to be dismal owing to its unfavorable conduction-band offset [48]. Similar to CIGSe, going to Zn(O,S) buffers will not improve the quality of the heterointerface, as they lead to worse lattice matching that would likely increase the surface recombination velocity. Therefore the Cd-free buffers in CZTSSe devices are expected to be limited by a higher S_h than those incorporating some fraction of Cd, but this limitation may be insignificant if they yield more controllable and advantageous CBOs and doping profiles with reduced absorption losses with respect to CdS-derived buffers.

D. Influence on dopability and the free carrier concentration

An added advantage to evaluating the branch-point energies is that they have previously been correlated with the concept of a CNL, i.e., a characteristic energy level associated with Fermi-level pinning in a material. The location of this level relative to the band edges has been remarkably successful in identifying a propensity for the observed conductivity in a variety of materials [25,27,49,50]. For n-type buffer layer partners to p-type absorbers like CIGSe or CZTSSe, it is therefore desirable to identify buffers in which the E_{BP} is closer to or even within the conduction band as compared to CdS.

Our results in Table II are consistent with previous reports that the E_{BP} or CNL fall within the conduction band for both CdO and ZnO and can qualitatively account for the robust and high n-type conductivity in these materials [25,49,51,52]. When combined with our calculated E_{BP}, this implies that incorporating some O into CdS or ZnS can have the effect of increasing a tendency for n-type conductivity, although the benefits to the carrier concentration cannot be completely decoupled from the influence of alloying on the band gap and also the band offsets as discussed in the next section.

We can attempt to approximately quantify this further by determining what carrier concentrations would be expected for a given value of the CNL. Specifically, we numerically determine the carrier concentration for a given Fermi level ϵ_F from the expression

$$n(\epsilon_F) = \frac{\sqrt{2}(m_e^*)^{3/2}}{\pi^2\hbar^3}\int_{E_{\mathrm{CBM}}}^{\infty} d\epsilon \frac{\sqrt{\epsilon - E_{\mathrm{CBM}}}}{1+e^{(\epsilon-\epsilon_F)/k_BT}}, \quad (3)$$

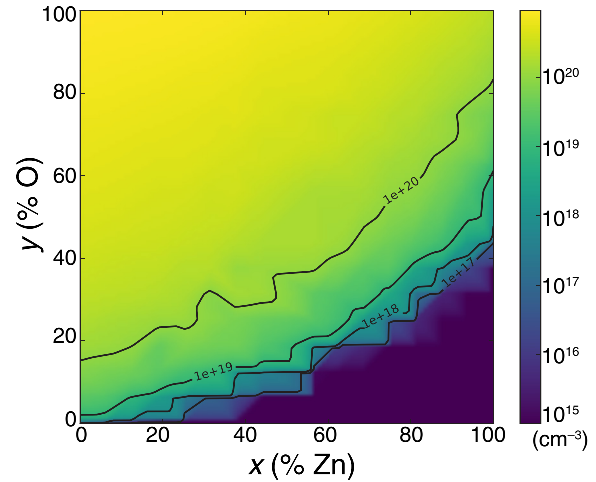

FIG. 2. Maps of the estimated free carrier concentrations as a function of composition based on the CNL pinning energy as described in the text (see Sec. III D).

where k_B is the Boltzmann constant, T is the temperature, m_e^* is the effective electron mass, ϵ is the electron energy, and E_{CBM} is the energy of the conduction-band edge. For the density of states effective masses, we linearly interpolate values for the alloys based on the composition and assuming values of 0.21, 0.21, 0.23, and 0.25 the mass of the free electron for CdS, CdO, ZnS, and ZnO, respectively. This analysis assumes a parabolic conduction band, but an extension to accounting for nonparaboilicity leads to only slightly larger carrier concentrations and does not influence our overall conclusions.

We include a map of estimated free carrier concentrations in Fig. 2 shown for 300 K and assuming upper bounds for the predicted Fermi-level pinning values 0.4 eV above the calculated E_{BP}. The plot captures the propensity for high n-type carrier concentrations achievable in CdO and ZnO ($>10^{19}$–10^{20} cm^{-3}), the modest concentrations in CdS (10^{16}–10^{17} cm^{-3}), and the generally poor dopability and n-type conductivity in ZnS. These results suggest that in addition to the possibility of improved interfaces with CIGSe, O incorporation into CdS may result in a greater tendency for obtaining higher carrier concentrations in the buffer if alloys can be realized over competing phases. For example, the simultaneous incorporation of sulfates and sulfites likely influences the effective conductivity of the buffer, as these phases are found to be energetically favorable (see Sec. III A) [19] and are expected to be electrically insulating due to their large band gaps [42]. Despite this issue, the prospect of alloy compositions that achieve suitable increases in carrier concentration compared to CdS can relax the constraints set on fine-tuning the CBO at the absorber-buffer interface [5]. These effects could translate to performance benefits that outweigh other consequences of alloying that may negatively influence the band gap and band offsets as discussed in the next sections.

E. Band gaps for reduced absorption losses

Identifying alternative buffers to CdS has been primarily motivated by the loss of valuable photocurrent in the blue

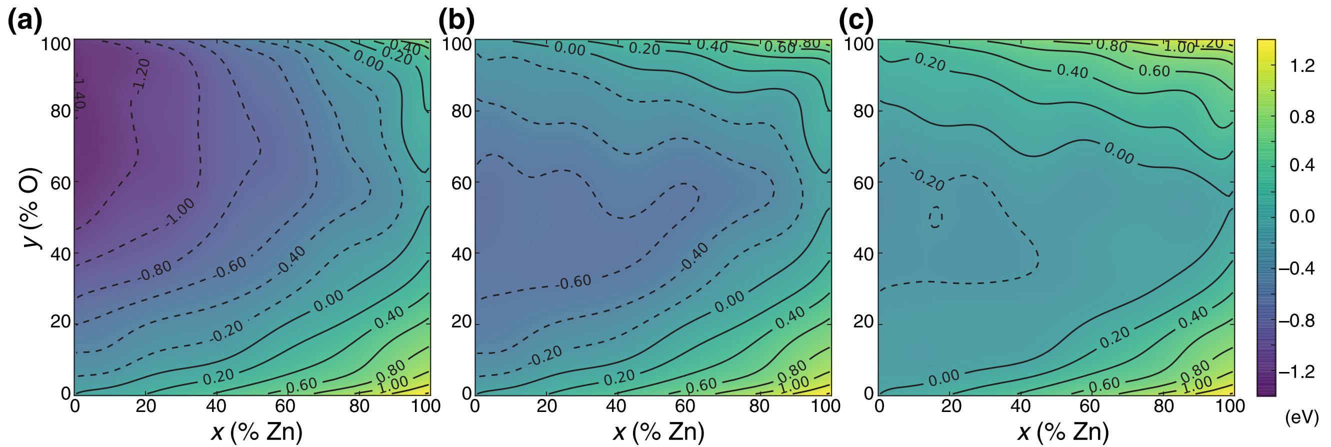

FIG. 3. Maps of the calculated fundamental (a) and estimated optical [(b) and (c)] band gaps for zinc-blende alloys shown as a function of the O and Zn content over the quaternary phase space (see Sec. III E for details). Due to the high carrier concentrations predicted for certain regions of the alloy space, we expect Burstein-Moss shifts in the optical absorption onsets as seen by the differences in (b) and (c) relative to (a). The optical band gaps are obtained by combining the fundamental band gaps (a) and the predicted Fermi pinning levels with respect to the CBMs from the calculated CNLs from the branch-point energies (b) and the hydrogen-related pinning levels (c) and offer reasonable bounds to estimate possible doping-induced blue shifts. The four corners in each panel represent the bulk references of CdS (lower left), CdO (upper left), ZnO (upper right), and ZnS (lower right).

portion of the solar spectrum. This has driven the development of Zn(O,S,OH) buffers, which are rapidly approaching comparable efficiencies to the record devices employing CdS buffers [38,42,46]. The push for larger-band-gap absorbers, which have the benefit of increasing V_{oc} linearly with the absorber band gap to first order and decreasing recombination in the space-charge and quasineutral regions [32], provides yet another reason for identifying better-suited buffer layer partners with the appropriate band gaps and offsets. For cases in which Cd-free buffers are not a requirement, the influence of Cd content on the band gap of Zn(O,S) alloys remains somewhat poorly understood and may prove advantageous in tuning the various relevant materials properties. Additionally, the possibility of collecting photocurrent from the buffer in the limit of high-quality interfaces and buffer material may offset the need for finding larger gap alternatives.

We include a contour map of the band gaps as a function of the O and Zn content in Fig. 3(a), where we define the gap as the energy difference between the highest-occupied and lowest-unoccupied Kohn-Sham single-particle states. Our results identify several composition regions that exhibit larger band gaps than pure CdS, which include more Zn-rich compositions and nearly the entire composition range of Zn(O,S) alloys. This is consistent with previous studies on (Cd,Zn)S alloys [53–56], and the growing interest in the Zn(O,S) alloys, which reduce unwanted absorption losses in the buffer. Our results suggest the incorporation of O into pure CdS leads instead to a redshift in the band gap, indicating the Cd(O,S) solid solutions should exhibit lower, and not larger band gaps in the zinc-blende and wurtzite phases. Reports of an increased band gap in polycrystalline or amorphous Cd(O,S) are likely attributed to the incorporation of other large-gap phases such as CdO_2, $CdSO_3$, and $CdSO_4$ rather than the formation of an oxysulfide solid solution [19,42,57]. This is supported by the recent experimental observation of a number of different large-gap sulfide and sulfite phases in oxygenated CdS buffers in CdTe devices [58,59] and the thermodynamics of the alloys [19].

We model the band gaps in the binary alloys using the expression

$$E_g(x) = (1-x)E_g^A + xE_g^B - bx(1-x), \tag{4}$$

where E_g^A and E_g^B are band gaps of the parent phases and b is known as the bowing parameter. The calculated bowing parameters are summarized in Table III alongside other reported experimental and theoretical values. As we describe below, the bowing parameters for the cation-site binary alloys were fit over the entire composition range, whereas the oxysulfides were fit over a range of intermediate compositions that does not include the dilute limit, which we explain below.

The observed behavior of the band gaps is found to exhibit a very nonlinear behavior, with the most pronounced band gap bowing occurring as a consequence of alloying on the anion site. This is consistent with previously reported bowing parameters summarized in Table III and the significantly smaller bowing parameters in the (Cd,Zn)O and (Cd,Zn)S systems compared to the oxysulfides. The large nonlinearities were previously identified in Zn(O,S) alloys both experimentally [60–62] and theoretically [63] and described within the band-anticrossing model (BAC). This model has been successful in describing the band gaps in highly mismatched alloys (HMA) where there is a significant interaction between the extended states of the host with the localized states of the isolelectronic anions in the dilute limit [62,64,65]. Therefore for these systems we only fit the expression for the band gaps with Eq. (4) for compositions from 5% to 95% for Zn(O,S) and Cd(O,S) similar to as in Ref. [63].

Our fit values over this range for Zn(O,S) ($E_g^{\mathrm{S}} = 3.72$ eV and $E_g^{\mathrm{O}} = 3.0$ eV and for the S-rich and O-rich limits) give a large bowing parameter of 3.41 eV and are in good agreement with values recently reported over a similar composition range

TABLE III. Summary of the calculated zinc-blende bowing parameters for the band gaps E_g and resolved into the conduction- and valence-band contributions for the binary references in the $Cd_{1-x}Zn_xO_yS_{1-y}$ quaternary space. All units are in eV.

Material	Cd(O,S)	Zn(O,S)	(Cd,Zn)O	(Cd,Zn)S
b	2.13	3.41	0.89	0.68
		3.0 [60,61], 3.61 [63]	0.94 [66],0.95 [67]	0.66 [68],0.61 [69]
			0.72–0.95 [70]	0.76 [56],0.91 [53–55]
b_v	1.74	2.88	0.26	0.17
b_c	0.62	1.14	0.63	0.51
E_g^S	2.41	3.72, 3.48 [63]	–	–
E_g^O	1.10	3.00, 2.78 [63]	–	–
E_S	2.45	4.02, 3.80 [63]	–	–
V_S	1.04	1.81, 2.44 [63]	–	–
E_O	1.14	3.23, 3.91 [63]	–	–
V_O	0.42	1.94, 3.91 [63]	–	–

in Ref. [63] that employed many-body perturbation theory to calculate the band gaps (see Table III). The calculated bowing parameters for Zn(O,S) are both overestimated compared to the reported experimental values of 3.0 eV, which is fit over the entire composition range [60,61]. If we had only fit Eq. (4) over the entire composition range, we would obtain a relatively poor fit and an even larger bowing parameter of approximately 4 eV. The BAC effects are smaller in Cd(O,S), where we calculate a $E_g^S = 2.41$ eV and $E_g^O = 1.10$ eV and a bowing parameter of $b = 2.13$ eV, which is close to the value of 2.23 obtained by fitting Eq. (4) over the entire composition range.

For the dilute anion alloys, we instead fit the band gap using the BAC model with an expression of the form [63]

$$E_g(x) = \tfrac{1}{2}\left(E_g^A + E_a - \sqrt{\left(E_g^A - E_a\right)^2 + 4xV_a^2}\right), \quad (5)$$

where we fit the parameters E_a and V_a and summarize our values in Table III for the O-rich and S-rich limits. As stated above, we fit Eq. (5) to a narrow range of compositions below 5% and above 95% O content for the oxysulfide alloys that are within the dilute alloy regime. Our values are in reasonable agreement with recent reports on Zn(O,S) alloys [63] and confirm the large impact on the electronic and optical properties of even dilute O (S) incorporation into ZnS (ZnO). The fits for Cd(O,S) indicate that the BAC effects are less pronounced in this material and that the standard band bowing expression in Eq. (4) is suitable for describing the band gap in these alloys over the entire composition range, while it fails for Zn(O,S) alloys.

We find that combining our independent binary bowing parameters from Table III into a two-dimensional band gap bowing function as in Ref. [71] leads to reasonably good agreement relative to the calculated band gaps. We find that the mean absolute error over the entire composition space is 0.09 eV with a standard deviation of 0.08 eV, with larger errors occurring for the band gaps of the compositions with an increasing amount of O and nearly equal concentrations of Cd and Zn. For example, the mean absolute error over compositions with less than 50% O is reduced to 0.07 eV with a standard deviation of 0.06 eV, indicating that the band gaps over many composition regions of interest can be accurately estimated from the independent parameters in Table III.

Fermi-level pinning within the conduction band is also indicative of a blue shift in the optical absorption threshold due to a Burstein-Moss shift and may also influence the effective band gap of the solid solution. These band-filling effects are well known to exist in CdO in its more stable rocksalt structure [51,72] and have also been identified in (Cd,Zn)O alloys [66,73]. We illustrate these effects in Figs. 3(b) and 3(c), which shows how band-filling from the high carrier concentrations that may be achievable in more Cd- and O-rich materials can lead to a larger effective optical gap. By comparing Figs. 3(a) and 3(b), a blue shift in the band gap is observed for buffers containing some O and also extends to combinations including some Zn, but it does not affect alloys without any O. This suggests that the incorporation of O could be beneficial to device performance in multiple ways through the predicted enhancement of dopability that may also lead to reduced absorption in the buffer. Futhermore, the results of Sec. III C suggest the improvements in the interfacial quality with some O incorporation may suppress the interfacial recombination to the point where a larger fraction of carriers generated within the buffer could be collected as photocurrent.

F. Band offsets for improved charge collection

A number of device simulation models and the form of Eq. (2) indicate that of all buffer-related parameters in a typical thin-film solar cell heterostructure, the CBO of the buffer with respect to the absorber and its degree of donor doping are most critical to maximizing performance [5,33,45]. These and other device model simulations indicate that a positive "spike" CBO ($< \sim$0.2–0.3 eV) with respect to the absorber leads to optimal V_{oc} for suitably n-type buffer materials, and that negative "cliff"-like offsets reduce the interfacial hole barrier ϕ_{0b} in Eq. (2) and lead to a linear decrease in V_{oc} with the decreasing CBO [5,31]. Interestingly, buffers with "cliff" CBOs within ~ -0.1 eV relative to the absorber were identified to yield high-performing devices for carrier concentrations routinely achieved in conventional CdS buffers ($\sim 10^{16}$–10^{17} cm^{-3}), and that even larger "cliff" CBOs may be tolerated if higher doping in the buffer can be achieved [5]. This illustrates the complexity of optimizing device performance and the importance of simultaneously tuning both the relative position

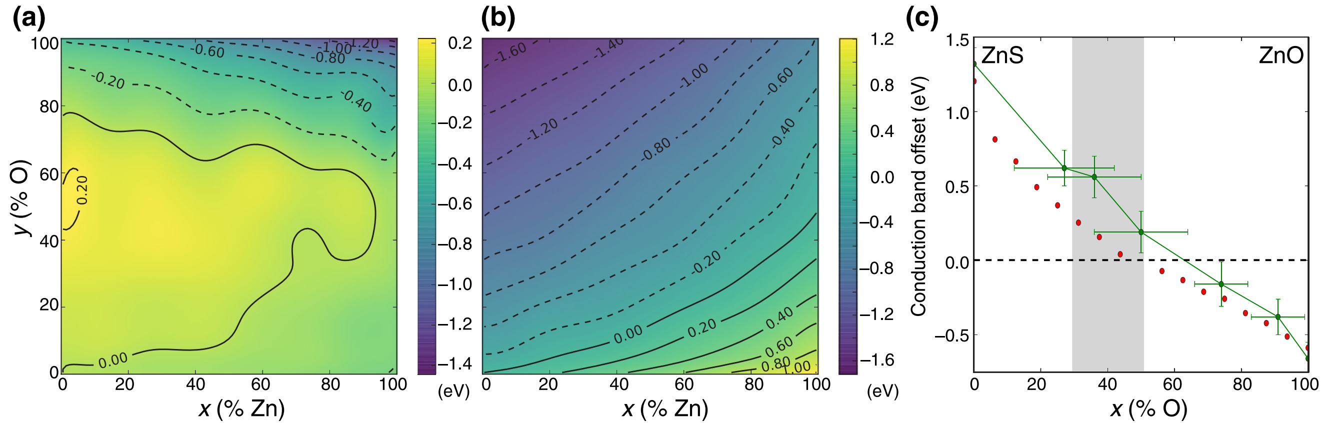

FIG. 4. Maps of the calculated valence-band (a) and conduction-band (b) offsets for zinc-blende alloys shown as a function of the O and Zn content relative to the pure CdS values (see Sec. III F). All values over the quaternary phase space assume the corrected band gaps and the branch-point energies as summarized in Table II and Fig. 3. The CBOs of the zinc-blende Zn(O,S) system relative to CdS are shown in (c), with experimental values extracted from Ref. [33] (green points) for ALD-grown films on Cu_2O with errors estimated from the reported O and S content. The conduction-band positions of the calculated and experimental data are both aligned to a CdS reference, which assumes transitivity holds for the Cu_2O/CdS and Cu_2O/Zn(O,S) heterojunctions. The region of 50%–70% S/(S+O) of Zn(O,S) is shaded as it is the typical composition range obtained in CBD-grown samples.

of the buffer conduction band and its degree of doping as described in Sec. III D.

We evaluate the influence of O and Zn incorporation on the band edges in Fig. 4, mapping the CBOs and also the valence-band offset (VBO) with respect to CdS. As described in Sec. II, we determine the VBO by evaluating the branch-point energy consistently for each reference structure, which defines a common energy level to evaluate the band positions. By combining the calculated VBOs with the band gaps for each composition [Fig. 3(a)], we are able to determine the CBOs. We can similarly use Eqs. (4) and (5) to fit the calculated offsets separately to resolve the contributions to the band gap bowing in terms of changes in the conduction and valence-band edges [74] and include the results in Table III.

Our results in Fig. 4 suggest that there is a fairly weak influence on the VBO over the majority of the composition space, with most changes in the band gap resulting from a shift of the conduction band. For example, we find the VBM of ZnS falls below that of CdS relative to the vacuum level by −0.18 to −0.22 eV depending on the phase, which agrees well with previously reported VBO values of ∼−0.1 to −0.2 eV based on experiment and theory [27,37,42,46,48,75,76]. This translates into a much larger influence on the conduction-band position for (Cd,Zn)S alloys, where nearly all of the difference in the band gap occurs in the cation-derived conduction band [10,27,37,55]. As the alloying of Ga into CIGSe has also been identified to nearly exclusively influence the position of conduction band, incorporating some Zn into CdS is one strategy to achieving more optimal conduction-band offsets with higher-Ga content CIGSe. However, this may come at the price of decreased doping efficiency as estimated in Fig. 2.

The exception to the relatively uniform valence-band position with composition corresponds to the strong influence of S incorporation into the oxide phases, consistent with the theory of HMAs [62]. We find that the large nonlinearities observed in the band gap bowing summarized in Table III for the oxysulfides reflects the sharp change in the valence-band positions of the oxide phases with a relatively small amount of incorporated S. Additionally, we find the magnitude of this bowing becomes enhanced with Zn incorporation. On the left side of Fig. 4(a), the overall valence-band offset spanning Cd(O,S) is highest for the pure oxide and spans −0.40 to −0.47 eV relative to CdS, depending on the phase, with a rapid change for S compositions of less than 5%. Our calculated VBOs spanning the Zn(O,S) are again highest for pure ZnO (−1.4 eV for zinc-blende and −1.56 eV for wurtzite ZnO relative to CdS) and are found to be somewhat larger than the ∼−1.0 to −1.3 eV extracted from theoretical estimates or experimental offsets of ZnO/CIGSe and assuming transitivity with CdS [27,42,46,75,76]. We find that the valence-band bowing in Zn(O,S) is also most severe for small sulfur concentrations below ∼10%, but that the decrease in the valence-band position begins at much higher S content (approximately 30% S) than in Cd(O,S), as seen in Fig. 4(a). The onset of this valence-band bowing is consistent with previous theoretical and experimental reports [62,77], while all of the studies differ in the magnitude of the changes.

From the standpoint of engineering better buffers, the influence of alloying on the valence band is only significant when combined with the band gaps to identify the resulting conduction-band offsets. We illustrate this for the Zn(O,S) system in Fig. 4(c), where we find that if the buffer becomes too O-rich, the CBO with respect to CdS becomes negative [33,62]. Our results identify the CBO for typical Zn(O,S) compositions accessible with CBD methods (∼50%–70% S)[42,46] exhibits either a small negative offset (∼−0.05 eV) to a positive offset (∼0.25 eV) relative to CdS over this range [see Fig. 4(c)]. Experimental reports on atomic-layer deposited Zn(O,S) films identified higher CBOs that fall over a range of ∼0.1–0.6 eV relative to CdS assuming transitivity with Cu_2O absorbers [33], while sputtered Zn(O,S) was predicted to have a lower CBO over this range and that aligned with CdS at 75% S content [62].

The sensitivity to O content combined with a relatively small window of compositions that yield CBOs comparable to CdS further emphasizes the need to establish better control over the exact composition of Zn(O,S). This is further complicated by the formation of different compounds that may be depend on the growth technique, such as the incorporation of sulfate, sulfite, and hydroxide phases in Zn(O,S) [19,46].

To put the obtained alloy band offsets in the context of CIGSe and CZTSSe absorbers we rely on transitivity and their reported offsets with respect to CdS. The most commonly reported theoretical value for the VBO of the CISe/CdS interface −1.07 eV, although experimental and theoretical values range from −0.6 to −1.36 eV with deviations due to different sample preparations, the existence of Cu-deficient surface phases, and details of the calculations such as crystallographic orientation, unrelaxed strain, or the presence of defects [10,31,37,42,46,78]. The influence of Ga content in CIGSe is expected to have little effect on the VBO with CdS, however, it has been shown that more Ga-rich interfaces result in larger offsets that approach the theoretical value due to the suppression of Cu-deficient surface phases [42]. Considering these facts and a large survey of reported values, Klein reported a value of −0.9 eV for the CIGSe/CdS valence-band offset [42], which is also consistent with the calculated VBO of ∼−0.8 eV for the Cu-deficient CISe/CdS interface [37]. Reported values for the VBO for CZTSe and CdS are −1.01 and −1.16 eV, respectively [76].

Combining the reported theoretical VBOs with the band gap values, the CBO of CdS is on the order of 0.3 eV for CISe and CZTSe, −0.4 eV for CGSe, and −0.1 eV for CZTS [37,42,76,78]. Neglecting the small bowing in CIGSe and CZTSSe alloys we can estimate a CdS CBO of 0.10 eV for typical low-Ga CIGSe (∼30% Ga) and 0.15 eV for CZTSSe (∼40% S), which both have band gaps of ∼1.2 eV [42,48]. If we instead adopt the −0.9 eV VBO for the CIGSe/CdS reported by Klein, we obtain a CBO of 0.30 eV [42]. We consider both of these values for the CIGSe/CdS band offsets in the device-level models in Sec. III H to account for the uncertainty, with the shifts in the band edges of the $Cd_{1-x}Zn_xO_yS_{1-y}$ alloys determined relative to CdS.

G. Identifying target compositions

Lastly, we combine all of the previously described criteria and choose a set of target properties of the buffer layer that we expect to improve performance. In Fig. 5(a), we establish a set of criteria for typical low-Ga CIGSe and CZTSSe alloys with band gaps around 1.2 eV. Our criteria, based on the fact that CdS buffers perform exceptionally well, are: (i) optical band gaps within −0.1 eV or larger compared to CdS to reduce absorption losses, (ii) a CBO within the range of −0.05 to 0.20 eV relative to CdS, and (iii) lattice match such that the interfacial recombination is greatly suppressed. The overlapping grey and blue regions in Fig. 5 are compositions that satisfy all three criteria. Combined with our estimates from Sec. III F, this translates into a CBO of 0.05–0.30 eV with respect to typical low-Ga CIGSe and 0.1–0.35 eV with respect to typical CZTSSe for a CISe/CdS VBO of 1.07 eV. Criterion (iii) also exhibits the possibility of offsetting the importance of (i) if the absorbed photons in the buffer also lead to carriers that can be efficiently collected.

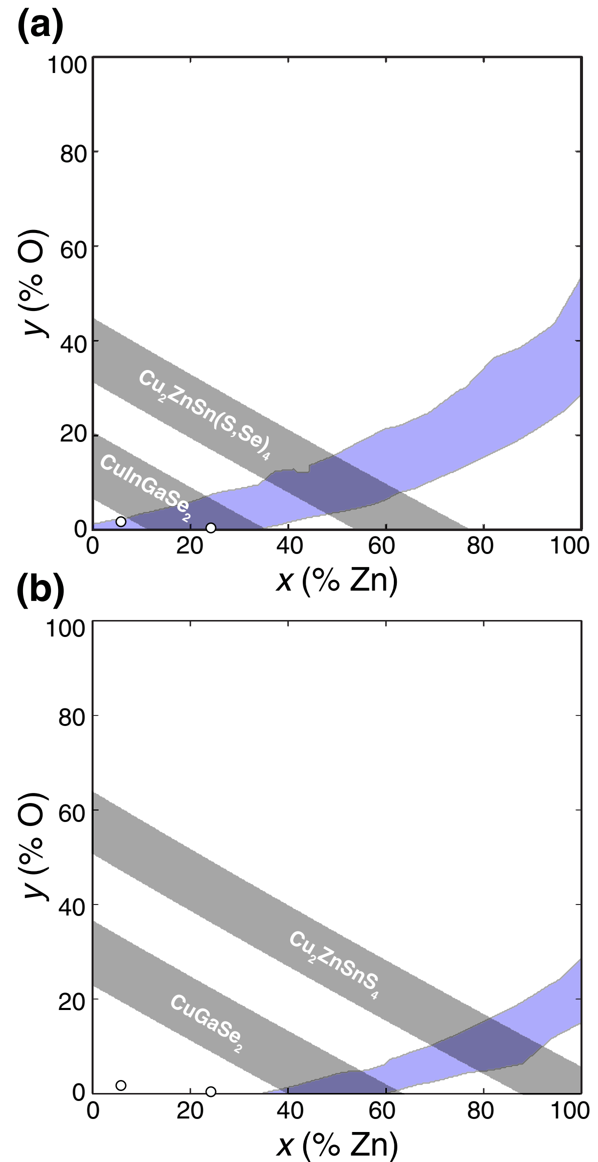

FIG. 5. A combination of all desired criteria in identifying target buffer compositions for a given absorber. In (a), we highlight compositions with blue shading that give an optical band gap within −0.1 eV or greater than CdS and a relative CBO −0.05−0.3 eV as would be desirable for typical CIGSe and CZTSSe alloys with band gaps ∼1.2 eV. The shaded grey bands indicate compositions that are lattice-matched within 1% to CIGSe and CZTSSe as in Fig. 1. In (b), we perform the same analysis with respect to the larger-band-gap absorbers of pure CGSe or CZTS, instead highlighting compositions with CBOs of 0.3 to 0.6 eV relative to CdS with blue shading. Compositions lattice-matched within 1% to CGSe and CZTS are again shaded in grey. The white points identify two of the compositions we focus on for the CIGSe device models in Sec. III H.

As seen in Fig. 5, our results identify a relatively small range of compositions that satisfy the criteria as a result of the large correlation between the conduction-band position and band gap in the $Cd_{1-x}Zn_xO_yS_{1-y}$ composition space. This strong correlation complicates the ability to independently tune the

band gap and conduction-band offset in these materials and results in a relatively narrow range of desirable compositions. This analysis identifies that ternary alloys like low-Zn content ($<\sim$35% Zn) (Cd,Zn)S alloys and moderate O-content ($\sim$50%–60% O) Zn(O,S) alloys would reduce absorption by the buffer while maintaining small "spike" CBOs relative to the absorber, based on transitivity with CdS. However, our results from Fig. 2 suggest that achieving suitable doping levels in (Cd,Zn)S buffer alloys may be more difficult than in the Zn(O,S) alloys [9,75,79], which could lead to diminished performance for their larger CBOs compared to CdS [5].

One strategy for sufficient n-type conductivity in these alloys may be doping with Al, which we have found to be a shallow donor in both CdS and ZnS [9,80] and which has proven an effective shallow donor dopant in ZnO, ZnS, and Zn(O,S) as well [81,82]. Simple estimates of the transition levels across the (Cd,Zn)S for common buffer donor dopants like In, Ga, and Al in the parent compounds would suggest Al would remain effective dopant for the entire alloy space, whereas In and Ga would become inefficient above $\sim$80% Zn content due to the larger ionization energies of these dopants in the Zn-rich limit [9,80]. Our results suggest this could be alleviated by the incorporation of some O into the (Cd,Zn)S alloys, which results in a larger range of $Cd_{1-x}Zn_xO_yS_{1-y}$ alloy compositions that satisfy the criteria as seen in Fig. 5.

In Fig. 5(a), we also include an additional requirement of lattice-matching to the absorber within 1%, which significantly reduces the possible compositions that satisfy all of the criteria as seen from the overlapping shaded regions. We note that this requirement is most likely to improve the S_h term in Eq. (2) as discussed previously, which only has a linear influence on the interfacial recombination rate, but it should increase the overall collection efficiency of light absorbed within the buffer. While compositions satisfying all criteria are desirable if possible, targeting compositions that yield a reasonable conduction-band position relative to the absorber is in general far more important for optimizing performance, as it determines both the CBO and dopability that are critical to minimizing the most significant terms in Eq. (2) [75].

In Fig. 5(b), we extend the analysis from the lower-gap absorbers to the higher-gap ones like pure CGSe or CZTS that may facilitate the development of tandem devices if their intrinsic defects can be controlled [43,44]. Here we instead choose compositions with a larger CBO within 0.3–0.6 eV relative to CdS to overcome the large "cliff"-type offsets expected for heterojunctions between CdS and CGSe. These choices translate into buffer CBOs ranging from -0.05 to 0.25 eV relative to CGSe. Again, (Cd,Zn)S alloys make up a large region of the compositions that meet the criteria, as do Zn(O,S) alloys with an O content ranging from $\sim$15%–30%. These compositions of Zn(O,S) are on the lower side of O content that is typically accessible with CBD growth but may be more readily achieved by other deposition techniques like sputtering, PVD, or ALD [33,60–62]. Our results for the larger CBOs also necessarily imply a larger separation to the E_{BP} and thus a possible reduction in the efficacy of donor doping for these compositions. Because a reduction in the buffer's free carrier concentration would strongly limit the band bending at the heterointerface and impede charge collection, the dopability of these $Cd_{1-x}Zn_xO_yS_{1-y}$ compositions should be further investigated to determine their ultimate viability as candidate buffer partners for larger-gap absorbers.

H. Performance of predictions in device-level models

We attempt an initial integration of our alloy models into a device-level simulation to extract trends with Zn and O incorporation on performance. We choose two representative compositions highlighted in Fig. 5 that lend themselves to changing the buffer properties by (1) increasing the CBO and band gap with a slight decrease to the carrier concentration and by (2) increasing the doping of the buffer at the cost of a slight redshift of the band gap. The alloys we consider are $Cd_{0.75}Zn_{0.25}S$ for the former and the more dilute quaternary $Cd_{0.94}Zn_{0.06}O_{0.02}S_{0.98}$ alloy for the latter, which are both expected to lead to high quality interfaces with CIGS (see Fig. 5). We implement these effects directly by reducing the carrier recombination velocities at the absorber-buffer interface by half ($S_h = 1 \times 10^2$ and $S_e = 1 \times 10^3$ cm s^{-1}) [29] while simultaneously modifying the other buffer layer parameters such as the band gap, optical absorption, shallow donor concentration, and electron affinity corresponding to our calculated composition-dependent values. While we motivate the choices for the reduced interfacial recombination velocities based on the improved interface, we note that these changes lead to no impact on the overall performance relative to the initial model parameters from Ref. [29].

We include the results of our SCAPS simulations for the modified buffers and a reference device with a CdS buffer layer in Table IV. Our device level models adopt all of the materials parameters detailed in Ref. [29], and we also consider another device model (model 2) that assumes adjusted band offsets for the CIGSe/CdS and CIGSe/ZnO interfaces following the values reported by Klein and described in Sec. III F [42]. The second model instead assumes an electron affinity of 4.0 eV for CdS and 4.3 eV for the ZnO layers that translates into a larger CBO of 0.3 eV for the reference CdS/CIGSe interface compared to the 0.1 eV value in the model of Frisk. This allows us to test the sensitivity of the initial assumptions about the reference buffer/absorber CBO, which is one of the most sensitive parameters determining device performance.

To implement the $Cd_{0.75}Zn_{0.25}S$ buffer simulation, we increased the band gap to 2.69 eV, shifted the absorption threshold, and decreased the electron affinity by 0.21 eV relative to CdS. We additionally consider a decrease of the shallow donor concentration by half ($N_D = 2.5 \times 10^{17}$ cm^{-3}) as compensation is expected to be more severe as more Zn is incorporated into CdS [10] and the lower electron affinity may decrease doping efficacy [75]. Our results in Table IV indicate that the blue shift of the band gap leads to a higher J_{sc} compared to the CdS reference for both models studied. For model 1, we find that the larger gap and larger CBO of $Cd_{0.75}Zn_{0.25}S$ can also improve the fill-factor and device efficiency if the doping in the buffer can be maintained at the same level as in CdS. However, we find that the larger CBO with CIGSe for the $Cd_{0.75}Zn_{0.25}S$ in model 2 becomes too large for the carrier concentrations in the buffer [5], which leads to a decrease in the fill-factor that leads to lower overall performance with respect to CdS despite increases in both V_{oc} and J_{sc}. These simulations

TABLE IV. Summary of the measured open-circuit voltage V_{oc}, short-circuit current J_{sc}, fill-factor FF, and device efficiency η for device-level models adopting the specified buffer compositions. Results are shown for the two models based on Ref. [29] (model 1) and Ref. [42] (model 2) as described in the text, with modified buffer performance shown relative to the CdS reference. Specific details of other modifications to the device simulations are included in the second row, such as scaled shallow donor concentrations N_D or absorption coefficients α.

		$Cd_{0.75}Zn_{0.25}S$		$Cd_{0.94}Zn_{0.06}O_{0.02}S_{0.98}$				
Buffer	CdS	N_D	$N_D/2$	N_D	$2N_D$	$N_D/2,\alpha/2$	$\alpha/2$	$N_D,\alpha/2$
Model 1								
V_{oc} (meV)	717	+2	+2	+0	+0	+3	+2	+1
J_{sc} ($\frac{mA}{cm^2}$)	32.02	+1.03	+0.90	−0.56	− 0.57	+0.16	+0.37	+0.39
FF (%)	77.77	−0.42	−2.57	− 1.28	− 0.57	− 4.21	−1.13	− 0.47
η (%)	17.84	+0.74	−0.04	− 0.58	− 0.43	−0.8	+0.0	+0.15
Model 2								
V_{oc} (meV)	718	+2	+6	− 1	− 1	+1	+0	+0
J_{sc} ($\frac{mA}{cm^2}$)	32.19	+0.90	+0.88	−0.55	−0.56	+0.22	+0.37	+0.37
FF (%)	78.44	−5.43	−13.00	−0.11	+0.03	− 2.16	− 0.05	−0.07
η (%)	18.13	− 0.75	−2.47	−0.36	− 0.33	− 0.36	+0.20	+0.23

confirm that wider gap alloys like $Cd_{0.75}Zn_{0.25}S$ may be promising buffer alternatives if they can be suitably doped.

For the quaternary $Cd_{0.94}Zn_{0.06}O_{0.02}S_{0.98}$ alloy we instead decrease the band gap to 2.35 eV, shift the absorption threshold, double the shallow donor concentration ($N_D = 1 \times 10^{18}$ cm^{-3}), and increase the electron affinity by 0.10 eV relative to CdS. Our results in Table IV indicate that the decrease of the band gap associated with O incorporation into the solid solution leads to a reduction in virtually all performance metrics compared to the CdS reference for both models studied, with overall efficiencies dropping by ∼0.3%–0.5% relative to CdS buffers. However, the slightly positive enthalpy of mixing for O incorporation into the CdS-derived buffers [19] and the observation of sulfite and sulfate phases in Cd(O,S) [58,59] suggests that these alloys likely have larger gap incorporated phases like $CdSO_4$ that contribute to reducing the absorption in these materials [42,57].

We attempt to approximately model this effect in our $Cd_{0.94}Zn_{0.06}O_{0.02}S_{0.98}$ alloy by scaling the wavelength-dependent absorption coefficient by half while maintaining the other material parameters that would still govern electrical transport through the buffer [42]. As seen from Table IV, our results indicate that the combination of the electrical characteristics of the $Cd_{0.94}Zn_{0.06}O_{0.02}S_{0.98}$ solid solution alloy with increased transparency offered by the larger band gap, incorporated phases (i.e., sulfates) can result in higher performance compared to CdS for both models if the effective carrier concentration of the buffer can be maintained at similar or higher levels to CdS. While the overall efficiency gains are modest for our specific examples, they illustrate the importance and complexity of simultaneously optimizing the buffer layer conduction-band offsets, doping, and absorption. Despite the simplicity of the model, the results may offer an explanation for the improved performance of oxygenated CdS buffer layers that could benefit from the higher carrier concentrations and suitable band edge positions of Cd(O,S) solid solutions intermixed with other insulating phases that reduce the effective absorption coefficient of the buffer [42]. The ultimate realization of optimal oxysulfide buffer alternatives will require additional study to better understand how the $Cd_{1-x}Zn_xO_yS_{1-y}$ solid solutions and other incorporated sulfate and sulfite phases contribute to the overall electrical and optical properties.

IV. SUMMARY AND CONCLUSIONS

In conclusion we report on how alloying O and Zn into CdS can influence a number of properties desirable for optimal buffer layers in thin-film PV. Using hybrid functional calculations, we characterize how the band gap and band offsets of $Cd_{1-x}Zn_xO_yS_{1-y}$ solid solutions are influenced as a function of composition. Our results suggest that modest fractions of O and Zn into CdS can facilitate higher quality buffer-absorber interfaces that may be less prone to interfacial recombination, and that Zn(O,S) buffers are expected to generally suffer from larger interfacial recombination velocities than CdS in CIGSe-based photovoltaics. Similarly, CZTSSe devices employing these buffers are also expected to suffer from larger interfacial recombination velocities compared to CIGSe devices.

We highlight compositions that may be relevant for low-gap and high-gap absorbers in the CIGSe and CZTSSe systems and our results identify there is only a select range of $Cd_{1-x}Zn_xO_yS_{1-y}$ compositions that may simultaneously minimize interfacial recombination rates and absorption losses through lattice-matched buffers with desirable conduction-band offsets and optical band gaps. Our results also support that Zn(O,S) buffers are promising alternatives to CdS, but that they have a relatively narrow window of compositions that yield desirable CBOs to typical CIGSe and CZTSSe absorbers and greater control must be achieved over their composition and properties. Other promising alternatives include (Cd,Zn)S alloys if the doping can be controlled and O-containing quaternaries if the composition can be controlled to engineer improved transparency. By corroborating our results with device-level models, we confirm that this range of compositions should yield attractive buffer alternatives to CdS that can result in higher performing thin-film photovoltaics.

ACKNOWLEDGMENTS

This work was performed under the auspices of the U.S. Department of Energy at Lawrence Livermore National Laboratory under Contract No. DE-AC52-07NA27344 and funded by the Department of Energy office of Energy Efficiency & Renewable Energy (EERE) through the SunShot Initiative through collaborative Development Grants in Energy (BRIDGE) program.

[1] P. Jackson, D. Hariskos, E. Lotter, S. Paetel, R. Wuerz, R. Menner, W. Wischmann, and M. Powalla, Prog. Photovolt: Res. Appl. **19**, 894 (2011).
[2] M. A. Green, K. Emery, Y. Hishikawa, W. Warta, and E. D. Dunlop, Prog. Photovolt: Res. Appl. **22**, 701 (2014).
[3] S. H. Demtsu and J. R. Sites, in *Conference Record of the Thirty-first IEEE Photovoltaic Specialists Conference, 2005* (2005), pp. 347–350.
[4] S. Siebentritt, Sol. Energ. Mat. Sol. C **95**, 1471 (2011).
[5] N. M. Mangan, R. E. Brandt, V. Steinmann, R. Jaramillo, C. Yang, J. R. Poindexter, R. Chakraborty, H. H. Park, X. Zhao, R. G. Gordon, and T. Buonassisi, J. Appl. Phys. **118**, 115102 (2015).
[6] J. Heyd, G. E. Scuseria, and M. Ernzerhof, J. Chem. Phys. **118**, 8207 (2003); **124**, 219906 (2006).
[7] P. E. Blöchl, Phys. Rev. B **50**, 17953 (1994).
[8] G. Kresse and J. Furthmüller, Phys. Rev. B **54**, 11169 (1996); Comp. Mater. Sci. **6**, 15 (1996).
[9] J. B. Varley and V. Lordi, J. Appl. Phys. **116**, 063505 (2014).
[10] J. B. Varley and V. Lordi, Appl. Phys. Lett. **103**, 102103 (2013).
[11] A. Ashrafi and C. Jagadish, J. Appl. Phys. **102**, 071101 (2007).
[12] P. Rinke, A. Qteish, J. Neugebauer, C. Freysoldt, and M. Scheffler, New J. Phys. **7**, 126 (2005).
[13] Q. Yan, P. Rinke, M. Winkelnkemper, A. Qteish, D. Bimberg, M. Scheffler, and C. G. Van de Walle, Appl. Phys. Lett. **101**, 152105 (2012).
[14] O. Madelung, *Semiconductors: Data Handbook* (Springer Verlag, 2004).
[15] X. Q. He, G. Brown, K. Demirkan, N. Mackie, V. Lordi, and A. Rockett, IEEE J. Photovoltaics **4**, 1625 (2014).
[16] A. Walsh, S. Chen, S.-H. Wei, and X. G. Gong, Adv. Energy Mater. **2**, 400 (2012).
[17] T. Maeda, S. Nakamura, and T. Wada, Jpn. J. Appl. Phys. **50**, 04DP07 (2011).
[18] J. von Pezold, A. Dick, M. Friák, and J. Neugebauer, Phys. Rev. B **81**, 094203 (2010).
[19] J. B. Varley, X. He, A. Rockett, and V. Lordi, ACS Appl. Mater. Interfaces **9**, 5673 (2017).
[20] J. Tersoff, Surf. Sci. **168**, 275 (1986).
[21] C. Tejedor and F. Flores, J. Phys. C: Solid State Phys. **11**, L19 (1978).
[22] W. Mönch, J. Appl. Phys. **80**, 5076 (1996).
[23] C. G. Van de Walle and J. Neugebauer, Nature (London) **423**, 626 (2003).
[24] J. Robertson, J. Vac. Sci. Technol. A **31**, 050821 (2013).
[25] A. Schleife, F. Fuchs, C. Rödl, J. Furthmüller, and F. Bechstedt, Appl. Phys. Lett. **94**, 012104 (2009).
[26] M. Cardona and N.E. Christensen, Phys. Rev. B **35**, 6182 (1987).
[27] Y. Hinuma, A. Grüneis, G. Kresse, and F. Oba, Phys. Rev. B **90**, 155405 (2014).
[28] M. Burgelman, P. Nollet, and S. Degrave, Thin Solid Films **361-362**, 527 (2000).
[29] C. Frisk, C. Platzer-Björkman, J. Olsson, P. Szaniawski, J. T. Wätjen, V. Fjällström, P. Salome, and M. Edoff, J. Phys. D: Appl. Phys. **47**, 485104 (2014).
[30] G. Hanna, A. Jasenek, U. Rau, and H.-W. Schock, Thin Solid Films **387**, 71 (2001).
[31] U. Rau and H.-W. Schock, Appl. Phys. A **69**, 131 (1999).
[32] J. V. Li, S. Grover, M. A. Contreras, K. Ramanathan, D. Kuciauskas, and R. N. Noufi, Sol. Energ. Mat. Sol. C **124**, 143 (2014).
[33] R. E. Brandt, M. Young, H. H. Park, A. Dameron, D. Chua, Y. S. Lee, G. Teeter, R. G. Gordon, and T. Buonassisi, Appl. Phys. Lett. **105**, 263901 (2014).
[34] Y. Hinuma, F. Oba, and I. Tanaka, Phys. Rev. B **88**, 075319 (2013).
[35] X. He, J. Varley, P. Ercius, T. Erikson, J. Bailey, G. Zapalac, D. Poplavskyy, N. Mackie, A. Bayman, V. Lordi, and A. Rockett, IEEE J. Photovoltaics **6**, 1308 (2016).
[36] X. He, P. Ercius, J. Bailey, G. Zapalac, N. Mackie, A. Bayman, J. Varley, V. Lordi, and A. Rockett, in *2015 IEEE 42nd Photovoltaic Specialist Conference (PVSC)* (2015), pp. 1–3.
[37] Y. Hinuma, F. Oba, Y. Kumagai, and I. Tanaka, Phys. Rev. B **88**, 035305 (2013).
[38] N. Naghavi, D. Abou-Ras, N. Allsop, N. Barreau, S. Bücheler, A. Ennaoui, C. H. Fischer, C. Guillen, D. Hariskos, J. Herrero, R. Klenk, K. Kushiya, D. Lincot, R. Menner, T. Nakada, C. Platzer-Björkman, S. Spiering, A. N. Tiwari, and T. Törndahl, Prog. Photovolt: Res. Appl. **18**, 411 (2010).
[39] Y. Hinuma, F. Oba, Y. Kumagai, and I. Tanaka, Phys. Rev. B **86**, 245433 (2012).
[40] D. Liao and A. Rockett, Appl. Phys. Lett. **82**, 2829 (2003).
[41] D. Liao and A. Rockett, J. Appl. Phys. **93**, 9380 (2003).
[42] A. Klein, J. Phys.: Condens. Matter **27**, 134201 (2015).
[43] J. Pohl and K. Albe, Phys. Rev. B **87**, 245203 (2013).
[44] B. Huang, S. Chen, H.-X. Deng, L.-W. Wang, M. A. Contreras, R. N. Noufi, and S.-H. Wei, IEEE J. Photovoltaics **4**, 477 (2014).
[45] M. Gloeckler and J. R. Sites, Thin Solid Films **480–481**, 241 (2005).
[46] T. Adler, M. Botros, W. Witte, D. Hariskos, R. Menner, M. Powalla, and A. Klein, Phys. Status Solidi A **211**, 1972 (2014).
[47] W. Wang, M. T. Winkler, O. Gunawan, T. Gokmen, T. K. Todorov, Y. Zhu, and D. B. Mitzi, Adv. Energy Mater. **4**, 1301465 (2013).
[48] D. A. R. Barkhouse, R. Haight, N. Sakai, H. Hiroi, H. Sugimoto, and D. B. Mitzi, Appl. Phys. Lett. **100**, 193904 (2012).
[49] P. D. C. King and T. D. Veal, J. Phys.: Condens. Matter **23**, 334214 (2011).
[50] S. B. Zhang, J. Phys.: Condens. Matter **14**, R881 (2002).

[51] M. Burbano, D. O. Scanlon, and G. W. Watson, J. Am. Chem. Soc. **133**, 15065 (2011).
[52] D. T. Speaks, M. A. Mayer, K. M. Yu, S. S. Mao, E. E. Haller, and W. Walukiewicz, J. Appl. Phys. **107**, 113706 (2010).
[53] A. Kuroyanagi, Thin Solid Films **249**, 91 (1994).
[54] W. Xia, J. A. Welt, H. Lin, H. N. Wu, M. H. Ho, and C. W. Tang, Sol. Energ. Mat. Sol. C **94**, 2113 (2010).
[55] J.-C. Wu, J. Zheng, C. L. Zacherl, P. Wu, Z.-K. Liu, and R. Xu, J. Phys. Chem. C **115**, 19741 (2011).
[56] J.-D. Huang, J.-Y. Liu, and K.-L. Han, Int. J. Hydrogen Energy **37**, 17870 (2012).
[57] X. Wu, R. G. Dhere, Y. Yan, I. J. Romero, Y. Zhang, J. Zhou, C. DeHart, A. Duda, C. Perkins, and B. To, in *Conference Record of the Twenty-Ninth IEEE Photovoltaic Specialists Conference, 2002* (2002), pp. 531–534.
[58] D. A. Duncan, J. M. Kephart, K. Horsley, M. Blum, M. Mezher, L. Weinhardt, M. Häming, R. G. Wilks, T. Hofmann, W. Yang, M. Bär, W. S. Sampath, and C. Heske, ACS Appl. Mater. Interfaces **7**, 16382 (2015).
[59] D. M. Meysing, C. A. Wolden, M. M. Griffith, H. Mahabaduge, J. Pankow, M. O. Reese, J. M. Burst, W. L. Rance, and T. M. Barnes, J. Vac. Sci. Technol. A **33**, 021203 (2015).
[60] B. K. Meyer, A. Polity, B. Farangis, Y. He, D. Hasselkamp, T. Krämer, and C. Wang, Appl. Phys. Lett. **85**, 4929 (2004).
[61] L. Zhang, L. Li, L. Wang, M. Li, Y. Lu, B. K. Meyer, and Y. He, J. Alloys Compd. **617**, 413 (2014).
[62] M. Jaquez, K. M. Yu, M. Ting, M. Hettick, J. F. Snchez-Royo, M. Wena, A. Javey, O. D. Dubon, and W. Walukiewicz, J. Appl. Phys. **118**, 215702 (2015), .
[63] G. Baldissera and C. Persson, J. Appl. Phys. **119**, 045704 (2016).
[64] M. Ting, R. dos Reis, M. Jaquez, O. D. Dubon, S. S. Mao, K. M. Yu, and W. Walukiewicz, Appl. Phys. Lett. **106**, 092101 (2015).
[65] M. A. Mayer, D. T. Speaks, K. M. Yu, S. S. Mao, E. E. Haller, and W. Walukiewicz, Appl. Phys. Lett. **97**, 022104 (2010).
[66] D. M. Detert, S. Lim, K. Tom, A. V. Luce, A. Anders, O. D. Dubon, K. M. Yu, and W. Walukiewicz, Appl. Phys. Lett. **102**, 232103 (2013).
[67] X. J. Wang, I. A. Buyanova, W. M. Chen, M. Izadifard, S. Rawal, D. P. Norton, S. J. Pearton, A. Osinsky, J. W. Dong, and A. Dabiran, Appl. Phys. Lett. **89**, 151909 (2006).
[68] M. C. Baykul and N. Orhan, Thin Solid Films **518**, 1925 (2010).
[69] J. Cizeron and M. P. Pileni, J. Phys. Chem. **99**, 17410 (1995).
[70] A. Schleife, C. Rödl, J. Furthmüller, and F. Bechstedt, New J. Phys. **13**, 085012 (2011).
[71] O. E. Jaime-Acuña, H. Villavicencio, J. A. Díaz-Hernández, V. Petranovskii, M. Herrera, and O. Raymond-Herrera, Chem. Mater. **26**, 6152 (2014).
[72] A. Segura, J. F. Sánchez-Royo, B. García-Domene, and G. Almonacid, Appl. Phys. Lett. **99**, 151907 (2011).
[73] W.-J. Yin, L. Dai, L. Zhang, R. Yang, L. Li, T. Guo, and Y. Yan, J. Appl. Phys. **115**, 023707 (2014).
[74] J. B. Varley, A. M. Conway, L. F. Voss, E. Swanberg, R. T. Graff, R. J. Nikolic, S. A. Payne, V. Lordi, and A. J. Nelson, Phys. Status Solidi B **252**, 1266 (2015).
[75] S. B. Zhang, S. Wei, and A. Zunger, J. Appl. Phys. **83**, 3192 (1998).
[76] S. Chen, A. Walsh, J.-H. Yang, X. G. Gong, L. Sun, P.-X. Yang, J.-H. Chu, and S.-H. Wei, Phys. Rev. B **83**, 125201 (2011).
[77] C. Persson, C. Platzer-Björkman, J. Malmström, T. Törndahl, and M. Edoff, Phys. Rev. Lett. **97**, 146403 (2006).
[78] S.-H. Wei and A. Zunger, Appl. Phys. Lett. **63**, 2549 (1993).
[79] W. Walukiewicz, Physica B **302–303**, 123 (2001).
[80] J. B. Varley, V. Lordi, X. He, and A. Rockett, J. Appl. Phys. **119**, 025703 (2016).
[81] H. H. Park, A. Jayaraman, R. Heasley, C. Yang, L. Hartle, R. Mankad, R. Haight, D. B. Mitzi, O. Gunawan, and R. G. Gordon, Appl. Phys. Lett. **105**, 202101 (2014).
[82] J. Bosco, F. Tajdar, and H. Atwater, in *2012 38th IEEE Photovoltaic Specialists Conference (PVSC)* (IEEE, 2012), pp. 002513–002517.